ACS OMEGA

http://pubs.acs.org/journal/acsodf

Article

Magnesium Polymer Electrolytes Based on the Polycarbonate Poly(2-butyl-2-ethyltrimethylene-carbonate)

David A. Sundermann, Bumjun Park, Valerian Hirschberg, Jennifer L. Schaefer, and Patrick Théato*

Cite This: *ACS Omega* 2023, 8, 23510−23520

Read Online

ACCESS | Metrics & More | Article Recommendations | Supporting Information

ABSTRACT: Magnesium electrolytes based on a polycarbonate with either magnesium tetrakis(hexafluoroisopropyloxy) borate ($Mg(B(HFIP)_4)_2$) or magnesium bis(trifluoromethanesulfonyl)-imide ($Mg(TFSI)_2$) for magnesium batteries were prepared and characterized. The side-chain-containing polycarbonate, poly(2-butyl-2-ethyltrimethylene carbonate) (P(BEC)), was synthesized by ring opening polymerization (ROP) of 5-ethyl-5-butylpropane oxirane ether carbonate (BEC) and mixed with $Mg(B(HFIP)_4)_2$ or $Mg(TFSI)_2$ to form low- and high-salt-concentration polymer electrolytes (PEs). The PEs were characterized by impedance spectroscopy, differential scanning calorimetry (DSC), rheology, linear sweep voltammetry, cyclic voltammetry, and Raman spectroscopy. A transition from classical salt-in-polymer electrolytes to polymer-in-salt electrolytes was indicated by a significant change in glass transition temperature as well as storage and loss moduli. Ionic conductivity measurements indicated the formation of polymer-in-salt electrolytes for the PEs with 40 mol % $Mg(B(HFIP)_4)_2$ (**HFIP40**). In contrast, the 40 mol % $Mg(TFSI)_2$ PEs showed mainly the classical behavior. **HFIP40** was further found to have an oxidative stability window greater than 6 V vs Mg/Mg^{2+}, but showed no reversible stripping-plating behavior in an Mg||SS cell.

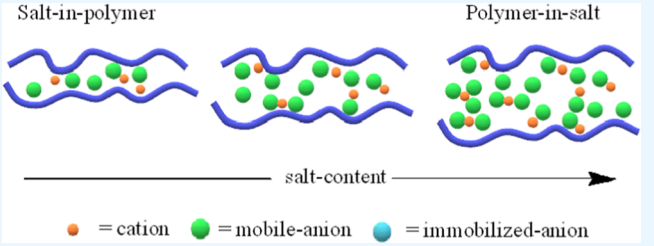

INTRODUCTION

In our digitized world, batteries have taken over a central task for many electric and mobile devices: energy storage. Batteries power technologies with a wide range of scale and energy/power needs, including the artificial cardiac pacemaker, smartphones, notebooks, and electrical vehicles (EVs).[1,2] Today's batteries are predominantly lithium ion batteries (LIBs), but the limited total global resources of lithium and the nonuniformity of the geography of lithium resources are drawbacks.[3] Therefore, other more common elements, including sodium, potassium, and magnesium, are being investigated for their use in rechargeable batteries.[4−6]

Magnesium is a more abundant material (5th most abundant) and has a higher volumetric capacity of 3823 mA h mL^{-1} compared to lithium (2061 mA h mL^{-1}).[7,8] Moreover, the recycling infrastructure for magnesium is more advanced than that for lithium, with recycling being a critical parameter for sustainability.[9−11] Besides all this, magnesium batteries still exhibit major drawbacks, including limited cycle life, large plating-stripping overpotentials, and a limited number of identified acceptable electrolytes.[12−14] The low compatibility of many electrolytes with magnesium metal anodes due to the formation of a nonconductive passivation layer that limits cyclability is arguably one of the main challenges. In addition, most studied magnesium electrolytes are based on flammable solvents. Therefore, the continued research of electrolytes for magnesium batteries, especially safer solid electrolytes, is warranted.

Polymer electrolytes (PEs) are generally found to have relatively large electrochemical stability windows and beneficial material properties and be low cost, but have limitations in ionic conductivities.[15] Magnesium ion batteries (MIBs) employing poly(ethylene glycol) (PEG), poly(vinylidene fluoride-hexafluoropropylene) (PVdF-HFP), poly(vinyl alcohol) (PVA), poly(vinyl pyrrolidone) (PVP), or poly(methyl methacrylate) (PMMA)-based electrolytes have been demonstrated.[16−19] Additional PE classifications are based on additives such as plasticizers, room-temperature ionic liquids (RT-ILs), or inorganic fillers. PEs with plasticizers and RT-ILs are summarized as gel-polymer electrolytes (GPEs) and those with fillers as composite polymer electrolytes (CPEs).[15] However, the performance of the reported solid polymer electrolytes for MIBs is still very poor; specifically, the stripping/plating efficiencies are low.[15] Polycarbonates are a well-studied class of PEs under study, with most reports focusing on polycarbonate electrolytes for LIBs and sodium-ion batteries (SIBs).[20−25] Various structural modifications were investigated, introducing aromatic moieties to improve the physical properties, but also side chains, e.g., ether-based or aliphatic side

Received: February 6, 2023
Accepted: May 19, 2023
Published: June 20, 2023

chains.[26−28] Aliphatic polycarbonates are in focus as solid PEs due to their amorphous structure, flexible chains, andelectrochemical and thermal stability.[29] The aliphatic polycarbonates include poly(ethylene carbonate) (PEC), pol(vinylene carbonate) (PVC), poly(propylene carbonate) (PPC), poly(trimethylene carbonate) (PTMC), and poly(2-butyl-2-ethyltrimethylene carbonate) (P(BEC)).[20,27,30−32] Ebadi and coworkers investigated the effect of aliphatic side chains on the electrochemical and physical properties by measuring the DSC and ionic conductivity.[27] They reported a reduced glass transition temperature (T_g) through the incorporation of aliphatic side chains, whereas the ionic conductivity decreases because of a reduced percolation of ion coordination sites. Sun and colleagues reported PTMC-based electrolytes for LIBs to have lithium transference numbers (t_{Li^+}) of up to 0.8 and to support cycling in $LiFePO_4$||Li cells.[22] Similarly, a sodium-ion PTMC electrolyte was reported to have a t_{Li^+} of 0.47 at 80 °C and support the cycling of CMC-Na||$Na_xFe[Fe(CN)_6]$ full cells for about 120 cycles.[24] Studies of polycarbonates in MIBs are in contrast to LIBs rare, with only a limited number of reports so far. Schaefer et al. reported on the characterization of poly(ε-caprolactone)-*co*-poly(trimethylene carbonate) with $Mg(TFSI)_2$, in comparison with the lithium electrolytes analog, toward its coordination assessment by impedance spectroscopy.[33] This electrolyte was not found to support reversible Mg metal plating and stripping, and identification of the contribution of the magnesium transport to the total ionic conductivity by Mg metal passivation. Aziz and colleagues reported on PEs composed of $Mg(TFSI)_2$ or magnesium perchlorate ($Mg(ClO_4)_2$) in poly(ethylene carbonate) (PEC), reporting ionic conductivities of up to 5.2×10^{-5} S cm^{-1} for 40 mol % $Mg(ClO_4)_2$ and high ion dissociation.[34]

The choice of magnesium salt has apparently important implications for the electrolyte performance, especially with regard to anode and cathode compatibility. Employing $Mg(TFSI)_2$ as salt is disadvantageous due to its propensity to passivate the magnesium metal anodes, as the $MgTFSI^+$ species will decompose at the magnesium anode during plating.[35−37] The boron-based salt $Mg(B(HFIP)_4)_2$ was developed as an alternative to $Mg(TFSI)_2$. Tuerxun and colleagues showed lower overpotentials, a higher reduction stability, and a higher coulombic efficiency for magnesium depositions and dissolution for a $Mg(B(HFIP)_4)_2$/triglyme solution than for $Mg(TFSI)_2$/triglyme.[38] Zhao-Karger and co-workers reported on the compatibility and performance of the $Mg(B(HFIP)_4)_2$-based liquid electrolytes for magnesium-sulfur batteries.[39] More recently, $Mg(B(HFIP)_4)_2$-ethereal solvent electrolytes were found by density functional theory (DFT) simulations to be sufficient electrolytes.[40] The simulations recommended a high oxidation stability and low interaction energy afforded by the CF_3 groups.

Polymer-in-salt electrolytes have recently gained more research interest. In polymer-in-salt electrolytes the polymer content is low, while a high salt content (exceeding 50 wt %) is present.[41] Their most prominent property is, for select polymer and salt combinations, improved ionic conductivity compared with conventional PEs.[42] To explain the relatively high ionic conductivity, several authors have proposed mechanisms such as ion transport through percolated ion aggregates (Mishra et al.) or by infinite cluster formation of aggregates (Bushkova et al.).[43,44] Polymer-in-salt electrolytes based on polymers with low T_g's such as PEC and PAN-based materials have been reported for lithium ion batteries, but no reports were published for MIBs as far as we know.[42,45,46]

Here, we report on magnesium polymer electrolytes based on P(BEC). P(BEC) was combined with either $Mg(B(HFIP)_4)_2$ or $Mg(TFSI)_2$ at concentrations of 5, 20, 30, and 40 mol %, and the resulting electrolytes were characterized by Raman spectroscopy, DSC, rheology, impedance spectroscopy, and cyclic voltammetry (CV). We find a polymer-in-salt electrolyte behavior, particularly in the case of 40 mol % $Mg(B(HFIP)_4)_2$. Further, an oxidative stability up to 6 V was measured by linear sweep voltammetry (LSV) next to a reversible stripping-plating behavior for about 5 cycles with 40 mol % $Mg(B(HFIP)_4)_2$ PE.

MATERIALS AND METHODS

Materials. All chemicals and solvents, unless otherwise stated, were used without further purifications. Ethylchloroformate (97%), trimethylamine (>99%), 2-butyl-2-ethyl-1,3-propanediol (99%), hexylamine (99%), 3,5-bis-(trifluoromethyl)phenyl isothiocyanate (>98%), and calcium hydride (95%) were purchased from Sigma-Aldrich. $Mg(TFSI)_2$ was dried at 200 °C under vacuum before use and stored under argon atmosphere. Tetrahydrofuran (THF, anhydrous, 99.9%) was dried with molecular sieves for at least a day before use. The solvent for $Mg(B(HFIP)_4)_2$ synthesis, 1,2-dimethoxyethane (DME, 99.5%, inhibitor free), was stored over Na metal for a week, distilled under N_2 atmosphere, and then dried with molecular sieves for a week in the glovebox prior to use.[47]

General Considerations. *Monomer Synthesis (2-Butyl-2-ethyltrimethylene Carbonate (BEC)).* 1 equiv 2-butyl-2-ethyl-1,3-propanediol (25 g, 156 mmol) was dissolved in 400 mL of dry THF at 0 °C under inert gas. After adding 2 equiv ethylchloroformate (29.8 mL, 312 mmol) to the mixture, 2 equiv triethylamine (43.2 mL, 312 mmol) in 200 mL of THF was added and the solution was stirred for 16 h at room temperature. The solution was filtered, concentrated, and redissolved in 400 mL of ethyl acetate. The organic layer was washed twice with 400 mL of 1 M HCl and twice with deionized water. The resulting product was purified by fractionated distillation under reduced pressure, resulting in a colorless liquid. Yield: 71%. ^{1}H NMR (400 MHz, $CDCl_3$) δ 0.63−1.05 (m, 6H), 1.05−1.54 (m, 8H), 4.1 (s, 4H).

Synthesis of 1-(3,5-Bis(trifluoromethyl)phenyl)-3-cyclohexylthiourea (TU). TU was synthesized as described in a previous report.[48] Yield: 85%. ^{1}H NMR (400 MHz, $CDCl_3$) δ 8.32 (s, 1H), 7.73 (m, 3H), 6.09 (s, 1H), 4.19 (s, 1H), 2.06 (m, 2H), 1.82−1.55 (m, 3H), 1.55−1.30 (m, 2H), 1.20 (m, 3H).

$Mg(B(HFIP)_4)_2$ Synthesis. $Mg(B(HFIP)_4)_2$ was synthesized as reported in the literature, and the product was obtained in the form of $Mg(B(HFIP)_4)_2$-3DME solids.[47] Yield: 87%. ^{1}H NMR (400 MHz, DMSO-d_6) δ 4.70 (s, CH3), 3.47 (s, CH_2), 3.28 (s, CH).^{19}F NMR (376 MHz, DMSO-d_6, H-decoupled) δ -74.3 (s, CF_3).

Poly(2-butyl-2-ethyltrimethylene carbonate) (P(BEC)) Synthesis. BEC (2 g, 10 mmol) was dissolved in dry DCM (5 mL) with TU catalyst (185 mg, 0.5 mmol) under inert gas. CaH_2 was added and the mixture stirred for 16 h. The solution was filtered afterward to remove solids and heated up to 30 °C before 1,8-diazabicyclo[5.4.0]undec-7-ene (DBU) (74.7 μL, 0.5 mmol) and benzyl alcohol (20.7 μL, 0.2 mmol) were added. After 24 h, the reaction was quenched by 1 mL of acetic acid and the polymer was precipitated into cold methanol two times. The polymer was dried for 24 h at 80 °C inside a glovebox before film preparation. ^{1}H NMR (400 MHz, $CDCl_3$) δ 7.34−7.26 (m,

https://doi.org/10.1021/acsomega.3c00761
ACS Omega 2023, 8, 23510−23520

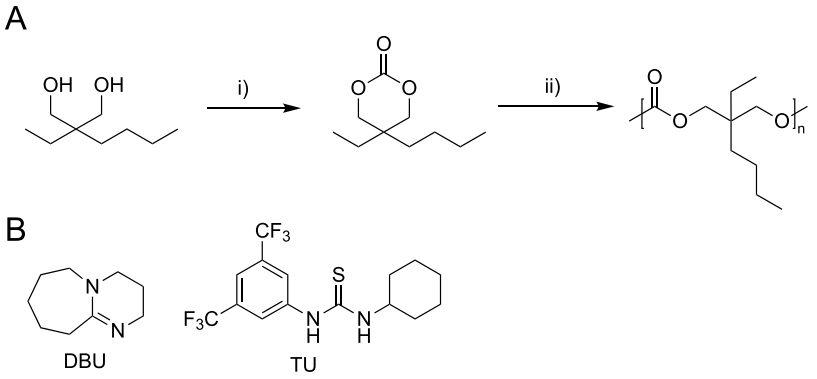

Figure 1. (A) Synthesis of P(BEC). Conditions: (i) ethylchloroformate, NEt_3, THF, 0 °C, 16 h. (ii) Benzyl alcohol, TU, DBU, DCM, 30 °C. (B) Structures of the cocatalysts DBU and TU.

1H), 3.93 (s), 1.33−1.06 (m), 0.90−0.72 (m). GPC M_n = 6100 g mol^{-1} ($Đ$ = 1.13).

General Polymer Electrolyte Film Preparation. $Mg(B(HFIP)_4)_2$-3DME and $Mg(TFSI)_2$ were combined with P(BEC) in THF at concentrations of 5, 20, 30, and 40 mol % magnesium salt to repeating unit, and electrolytes were prepared by solution casting under argon atmosphere. After the bulk solvent appeared to have evaporated, the electrolytes were dried for 24 h at room temperature under vacuum in an argon-filled glovebox, followed by 48 h at 80 °C.

Nuclear Magnetic Resonance Spectroscopy (NMR). NMR data were recorded with a Bruker Ascend 400 MHz NMR. The chemical shift for ^1H NMR spectra was reported in parts per million (ppm) referenced to the characteristic solvent signal of $CDCl_3$ at 7.26 ppm or DMSO-d_6 at 2.49 ppm.

Gel Permeation Chromatography (GPC). The samples were prepared in an THF eluent at a concentration of 1 mg mL^{-1} and analyzed over PSS SDV 5 μm columns and an IR detector with a Tosoh EcoSEC pump at 35 °C and an acquisition time of 35 min. PMMA reference material was used to estimate the molecular weight.

Differential Scanning Calorimetry (DSC). DSC measurements were conducted on a DSC Q2000 V24 in the range from −100 to 125 °C, with a scan rate of 10 K min^{-1} for all measurements (preheating step to 130 °C and precooling step to −100 °C before performing the measurement).

Thermogravimetric Analysis (TGA). TGA measurements were performed using TGA5500 from Waters, TA Instruments, with a temperature ramp of 10 °C per minute from 50 to 500 °C.

Raman Spectroscopy. Samples were prepared in an argon-filled glovebox and sealed in quartz cuvettes. Raman spectra were obtained using Jasco NRS-5100 with excitation laser with a wavelength of 532 nm. The signal was calibrated with a silicon wafer at a wavenumber of 520.7 cm^{-1}. Raman spectra were obtained with 5−10 scans for 1−2 min, which sums up to a total scan time of around 10 min.

Rheology Measurements. The rheological experiments were performed using a strain-controlled ARES-G2 rheometer (TA Instruments). For small-amplitude oscillatory shear (SAOS) measurements, parallel plates with a diameter of 13 mm were used, with temperature control using a Peltier at 20 °C. Oscillatory strain sweeps (γ_0 = 0.01−100%) at a constant angular frequency of ω = 6.28 rad s^{-1} were conducted to determine the linear viscoelastic regime (LVE), followed by oscillatory frequency sweeps. Strain amplitudes between γ_0 = 0.02 and 10% were chosen for the frequency sweeps, depending on the LVE of the blend.

Ionic Conductivity Measurements. Ionic conductivity was measured using a broadband dielectric spectrometer with an Alpha A analyzer, outfitted with a cryostat and a Quatro temperature control unit (Novocontrol Technologies, Montabaur, Germany). The previously prepared PE samples were sandwiched between two stainless-steel electrodes using a Mylar foil spacer ring (thickness l = 100 μm, inner diameter = 8 mm). Coin cells (CR2032) were assembled and aged at 120 °C overnight before measurement to improve contact between the electrodes and the electrolyte. Ionic conductivity was measured over a frequency range of 10^7−10^{-1} Hz with an amplitude of 10 mV, with a gradual increase in temperature from −10 to 120 °C in 10 °C steps and with a following reverse heating procedure cooled down to −10 °C. The temperature was stabilized at each point for 10 min within 0.5 °C prior to each measurement. For each polymer, at least three coin cells were measured to derive the average ionic conductivity.

Electrochemical Measurements. Electrochemical measurements were conducted using a PARSTAT MC1000 (Princeton Applied Research) potentiostat. Coin cells (CR2032) were assembled with the same spacer used for ionic conductivity measurement, wherein SS and Mg electrodes were used as working and counter electrodes.

Cyclic voltammetry (CV) measurements were performed between −2 to 2 V vs $Mg||Mg^{2+}$ for five cycles at 80 °C and a scan rate of 0.1 mV s^{-1}. Electrochemical impedance spectroscopy (EIS) measurements were conducted before and after CV measurements over a frequency range of 10^6−10^{-1} Hz with an amplitude of 10 mV at 80 °C.

Linear sweep voltammetry (LSV) measurements were performed at 20 °C between 0 and 6 V vs $Mg||Mg^{2+}$ at a scan rate of 0.1 mV s^{-1}.

RESULTS AND DISCUSSION

P(BEC) as aliphatic polycarbonate was taken due to its low T_g and high chain flexibility.[27] It was synthesized by anionic ring opening polymerization (ROP) as schematically shown in Figure 1A, using the cocatalysts DBU and TU. Using ^1H NMR spectroscopy, the degree of polymerization (average number of repeating units per chain) was calculated to be 22, by integrating and comparing the peak from the CH_2 of the benzyl alcohol at 5.07 ppm with the peak from the CH_2 groups of the repeating units at 3.93 ppm. Based on GPC measurements, an M_n = 6100 g mol^{-1}, equivalent to a degree of polymerization of 32, was estimated. Considering PMMA standards were used for calibration of the GPC, the GPC results confirmed the ^1H

https://doi.org/10.1021/acsomega.3c00761
ACS Omega 2023, 8, 23510−23520

NMR result of about 22 repeating units per polymer. Next, PEs were prepared by incorporating 5, 20, 30, and 40 mol % $Mg(TFSI)_2$ (**TFSI5** to **TFSI40**) or $Mg(B(HFIP)_4)_2$-3DME (**HFIP5** to **HFIP40**) into the polymer matrix by the solution casting method. All PEs were solid and/or gum-like materials.

Differential Scanning Calorimetry and Thermogravimetric Analysis. The polymer P(BEC) had a decomposition temperature (T_d) of 166 °C (Figure S9), which was in a similar range to that previously reported for polycarbonates.[34] The physical properties of the P(BEC) and the corresponding PEs were analyzed by DSC (Figure 2, Figures S6, S7 and Table 1),

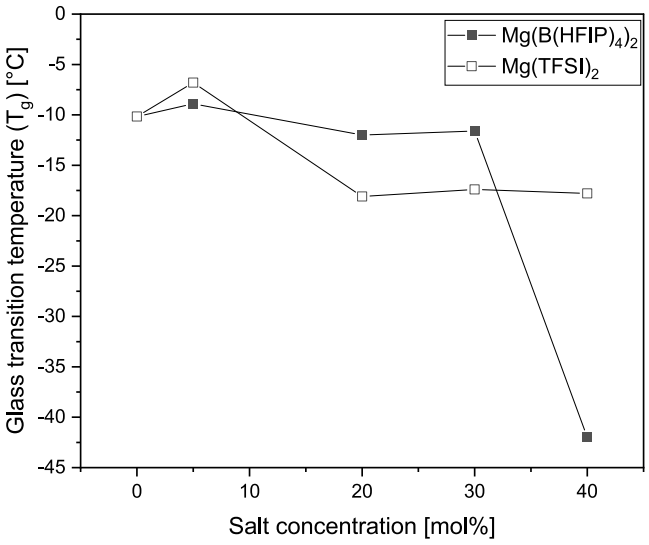

Figure 2. Glass transition temperatures of the studied P(BEC) electrolytes as a function of varying concentrations of magnesium salt measured for $Mg(TFSI)_2$ and $Mg(B(HFIP)_4)_2$.

detecting for the pure polymer a glass transition temperature (T_g) of −10 °C. The addition of 5 mol % $Mg(TFSI)_2$ (**TFSI5**) to the polymer matrix led to a slight increase in T_g to about −7 °C. For **TFSI20** to **TFSI40** the T_g decreased to about −17 °C, reaching a plateau, which indicated the formation of a stable phase being salt content independent. The decrease in T_g might be caused by the plasticizing effect of the $TFSI^-$ anion, as already reported elsewhere.[34,49] The addition of $Mg(B(HFIP)_4)_2$ led to a similar observation, where **HFIP5**, **HFIP20**, and **HFIP30** showed only a slight decrease in T_g from −9 to −12 °C but a sudden drop for **HFIP40** to −42 °C. This rapid change in T_g hinted at a significant change in phase, suggesting the formation of polymer-in-salt electrolytes for **HFIP40**. In previous studies, a significant decrease in T_g was already reported for PEs with salt contents larger than 50 wt %, which is traced back to the suppression of salt crystallization through the polymer-salt interaction.[50] Furthermore, no $Mg(B(HFIP)_4)_2$-3DME complexes remained after the PE preparation due to the absence of any melting point corresponding to the salt complex (Table 1).

Raman Spectroscopy. The anion coordination behavior was characterized by Raman spectroscopy. For $Mg(TFSI)_2$, we focused on analyzing the changes in the C−F vibrations between 740 to 760 cm^{-1} and the polymer C−H vibrations between 2800 to 3000 cm^{-1} (Figure 3).[51] The polymer was inactive in the area of 750 cm^{-1}, and therefore these signals belonged only to the $TFSI^-$, where a shift toward higher wavenumbers and energies can be seen by an increase in $Mg(TFSI)_2$ concentration. Two overlapping vibrations were suggested with maxima at 744 and 752 cm^{-1} corresponding to free $TFSI^-$ at 740 cm^{-1} and Mg^{2+}-coordinated $TFSI^-$ at 752 cm^{-1} as previously reported.[51] By fitting the curves to Gaussian functions, an increase of Mg^{2+}-coordinated TFSI from 35.1 to 76.0% can be seen (Table S1 and Figure 4) with increasing salt concentration from 5 to 40 mol % $Mg(TFSI)_2$. For the C−H vibrations, a slight shift toward higher wavenumbers (2964−2998 cm^{-1}) was also observed, indicating an increasing Mg−polymer interaction with increasing $Mg(TFSI)_2$ concentration.

An explanation considering both observations could be that in the first step, the complexation of Mg^{2+} by the polymer was preferred, leading to a higher salt dissociation for **TFSI5** and therefore less ion pairs or aggregates. With further increase in $Mg(TFSI)_2$ content, the formation of ion pairs or aggregates increased because the coordination sites on the polymer chains were occupied. Thus, the preferred coordination number of 6 for Mg^{2+} could not be fulfilled by P(BEC), promoting the formation of aggregates and ion pairs.[52] Therefore, the higher T_g for **TFSI5** was caused by a higher quasi-ionic cross-linking of the polymer by a higher number of polymer-Mg complexes due to higher $Mg(TFSI)_2$ dissociation. With further increase in $Mg(TFSI)_2$ content, the formation of ion pairs and aggregates occurred, reducing the quasi-ionic cross-linking and leading to a decrease in T_g.[49] Compared to a PEC-based magnesium PE published in 2018, the ratio of free $TFSI^-$ is significantly lower in P(BEC), where instead of 24% free $TFSI^-$, at 40 mol % 87% free $TFSI^-$ was reported.[34] This difference might be caused by the higher

Table 1. Salt Concentration, Glass Transition Temperature (T_g), and Ionic Conductivity (σ) at 20 °C of TFSI5 to TFSI40 and HFIP5 to HFIP40

	Mg/repeating unit [mol %]	salt concentration [wt %]	glass transition temperature T_g [°C]	σ at 20 °C [S cm^{-1}]
P(BEC)	0	0	−10	[a]
$Mg(TFSI)_2$	[a]	[a]	[b]	[a]
TFSI5	5	13.6	−7	2.7×10^{-7}
TFSI20	20	38.6	−18	6.4×10^{-9}
TFSI30	30	48.5	−17	1.0×10^{-9}
TFSI40	40	55.7	−18	5.4×10^{-10}
$Mg(B(HFIP)_4)_2$ 3DME	[a]	[a]	T_m at 51 and 96	[a]
HFIP5	5	27.1	−9	1.3×10^{-12}
HFIP20	20	59.8	−12	2.4×10^{-12}
HFIP30	30	69.0	−12	2.3×10^{-13}
HFIP40	40	74.8	−42	9.2×10^{-8}

[a]Assigned to not measured. [b]Not detected.

https://doi.org/10.1021/acsomega.3c00761
ACS Omega 2023, 8, 23510−23520

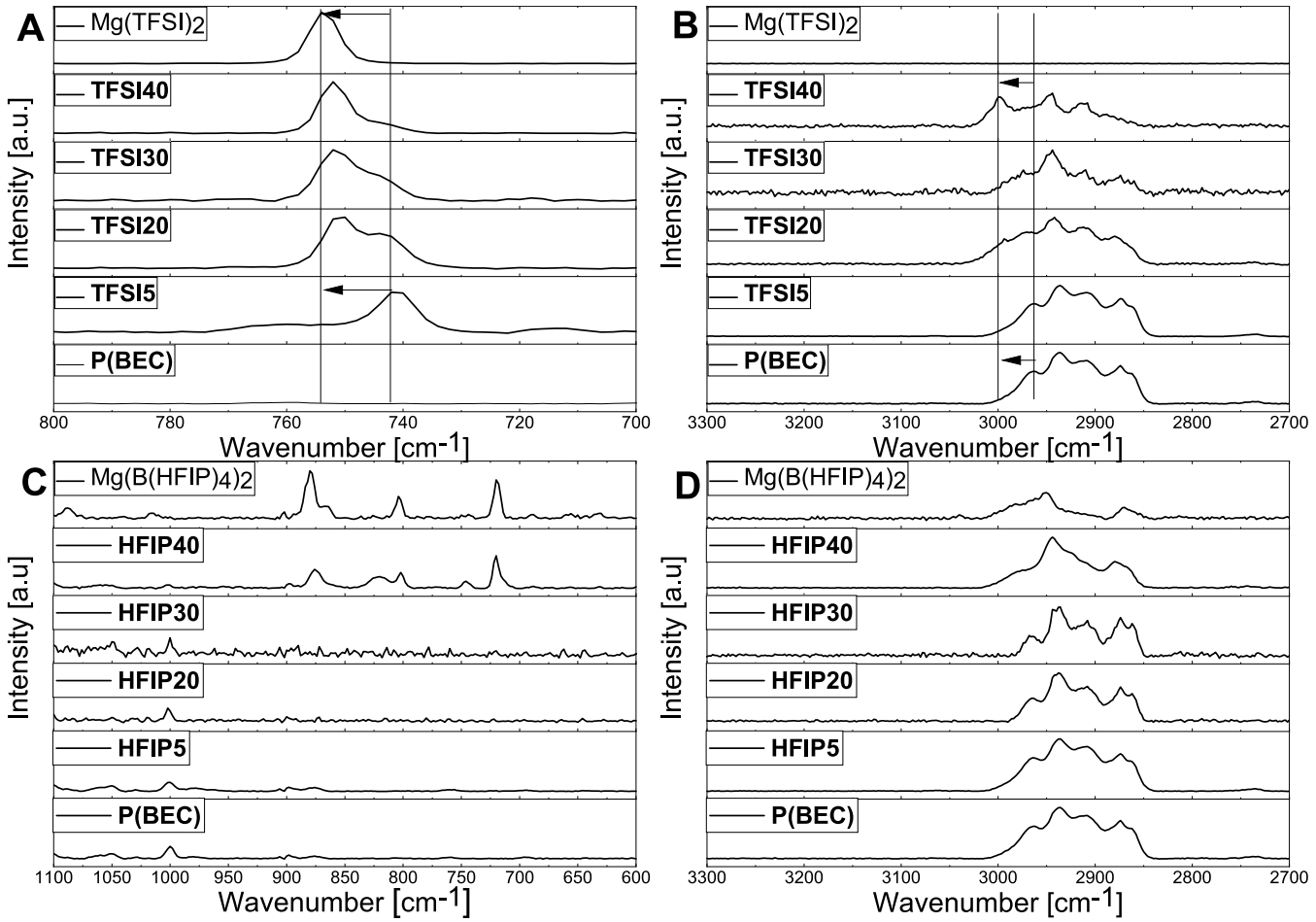

Figure 3. Raman spectra of (A, B) **TFSI5** to **TFSI40** and (C, D) **HFIP5** to **HFIP40**.

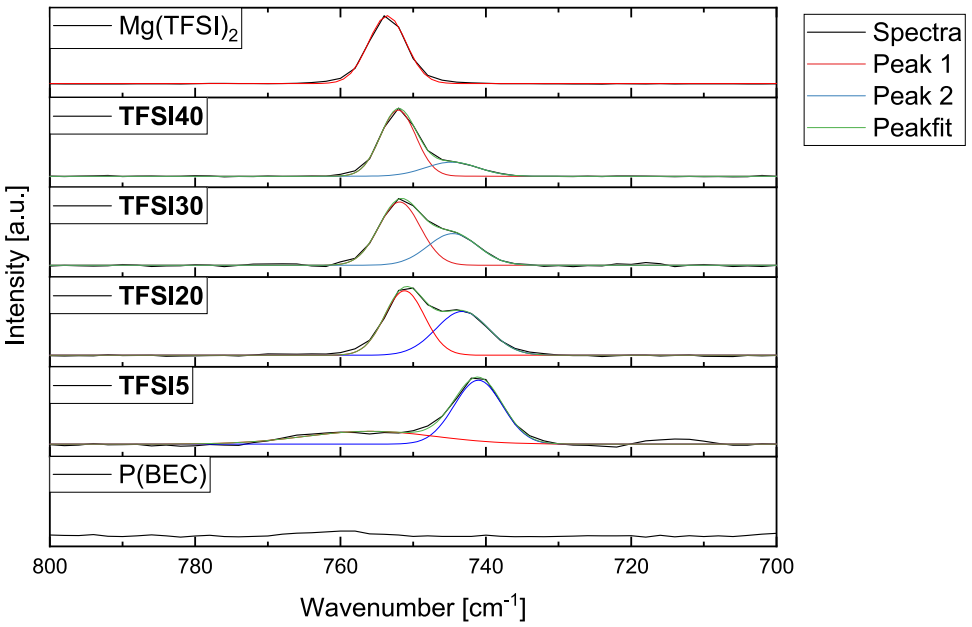

Figure 4. Raman spectra between 800 to 700 cm^{-1} with fitted peaks 1 and 2.

aliphatic character and therefore smaller dipole moment of P(BEC), compared to PEC enhancing the formation of ion pairs and aggregates.[53]

In contrast to $Mg(TFSI)_2$, no significant shifts in the Raman spectra between 2800 to 3000 cm^{-1} were observed for the $Mg(B(HFIP)_4)_2$-containing PEs. $Mg(B(HFIP)_4)_2$-3DME was Raman active in the area of 700 to 900 cm^{-1} (Figure 3), where

https://doi.org/10.1021/acsomega.3c00761
ACS Omega 2023, 8, 23510−23520

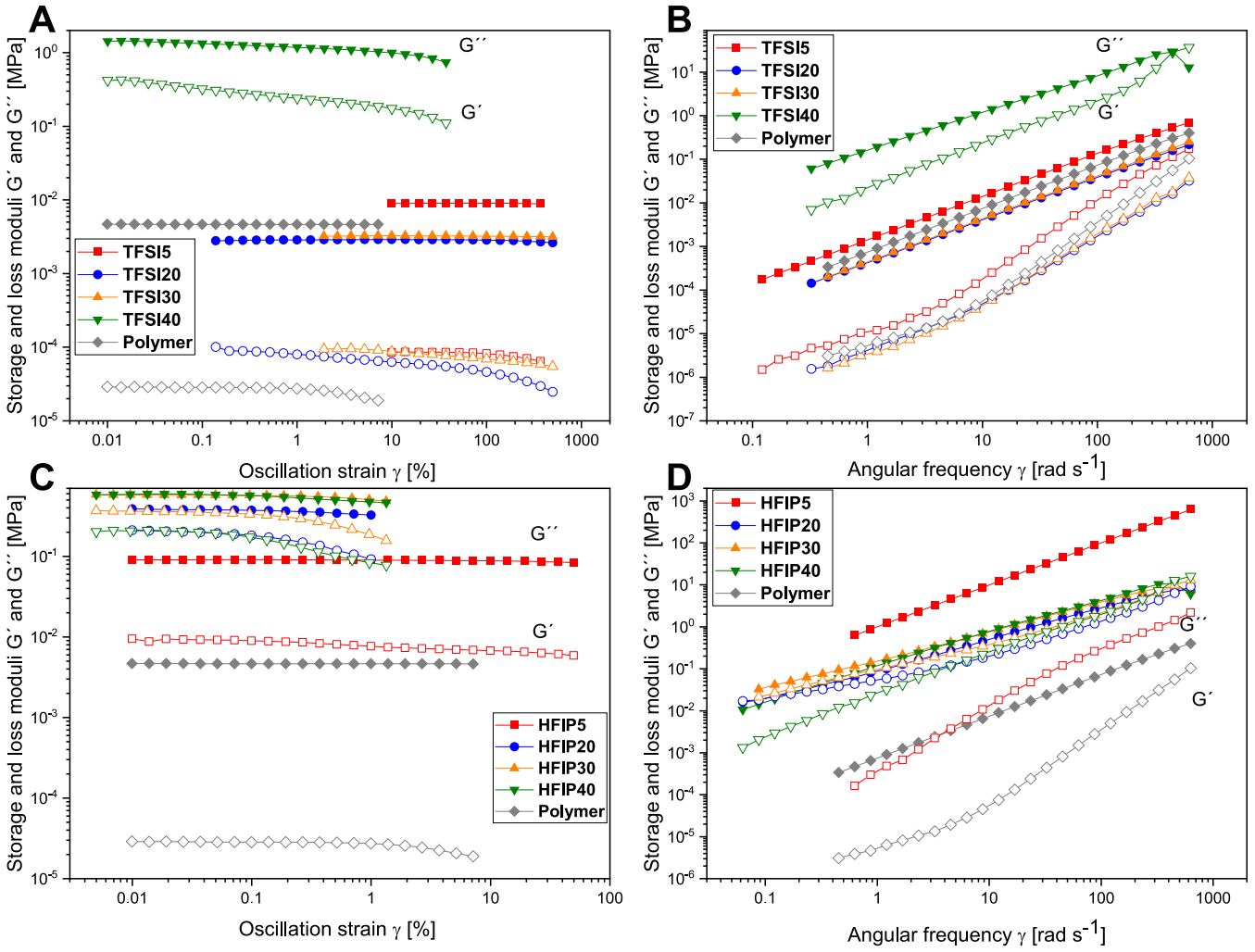

Figure 5. Rheological SST and DFS measurements at 20 °C with filled symbols for loss modulus G'' and empty symbols for storage modulus G' of (A, B) **TFSI5** to **TFSI40** and (C, D) **HFIP5** to **HFIP40** as well as the neat polymeric matrix.

vibration at 718 cm^{-1} and further vibrations at 804 and 880 cm^{-1} were detected. Based on previous reports, the vibrations at 880 cm^{-1} were C−O−C vibrations of DME, whereas the peaks at 804 and 718 cm^{-1} were assigned to B−O and C−F vibrations.[38] Overall those three signals only appeared for **HFIP40** without any shifting, but were missing for the electrolytes with less than 40 mol % $Mg(B(HFIP)_4)_2$, suggesting a complete solvation of the salt below 30 mol %. Because no shifts of the signals at 880, 804, and 718 cm^{-1} were seen, it is inferred that a precipitation of the $Mg(B(HFIP)_4)_2$-3DME salt occurred in **HFIP40**. The precipitation of salts was already observed in the literature for lithium salts, e.g., in poly(acrylonitrile-*co*-butyl acrylate) (P(AN-*co*-BuA)) at high salt contents.[45] However, the overall amount of DME and therefore $Mg(B(HFIP)_4)_2$-3DME in **HFIP40** is still suggested to be low due to the absence of any DME signals in ^1H NMR (Figure S10) or any further T_g or T_m by DSC. Moreover, the Raman results underline the combination with the DSC results the suggestion of a polymer-in-salt electrolyte for **HFIP40**.

Rheology. The given samples **TFSI5** to **TFSI40** and **HFIP5** to **HFIP40** were analyzed by the dynamic strain sweep test (SST) and dynamic frequency sweep (DFS) to determine the storage (G') and loss (G'') moduli, representing the elastic and viscous parts of the materials as functions of oscillation strain (γ) and angular frequency (ω). DFS studies were performed in the linear viscoelastic regime (LVE) with strain amplitudes between γ_0 = 0.02 and 10%. The PEs showed overall a complex rheological response, with the salt concentration and magnesium salt type being frequency dependent.

For SST measurements (Figure 5A,B), the loss modulus G'' was mostly dominant over the storage modulus G' for all PEs regardless of magnesium salts or concentrations, indicating more viscosity than elastic materials.[54]

Based on these results, complex viscosities (η^*) (Figure 6) were calculated at ω = 0.32 rad s^{-1} and γ_0 = 10% to compare the different blends. The complex viscosity η^* increased constantly with increasing $Mg(B(HFIP)_4)_2$ concentration, reaching its maximum for **HFIP30** and then slightly decreasing again for **HFIP40**. Earlier polymer-related publications, i.e., poly(ethylene-*co*-methacrylic acid), explained the increasing viscosity by an increase in ionic interaction, in this case as quasi-ionic cross-linking.[55,56] The increase in η^* can therefore also be related to the increasing quasi-ionic cross-linking for **HFIP5** to **HFIP30**. The decrease in η^* for **HFIP40** is attributed to the precipitation of salt and decrease in T_g of **HFIP40**. Similarly, the η^* trend of **TFSI5** to **TFSI30** can be explained, where η^* decreased due to a higher number of ion pairs and agglomerations and lower salt dissociation, as discussed before.

https://doi.org/10.1021/acsomega.3c00761
ACS Omega 2023, 8, 23510−23520

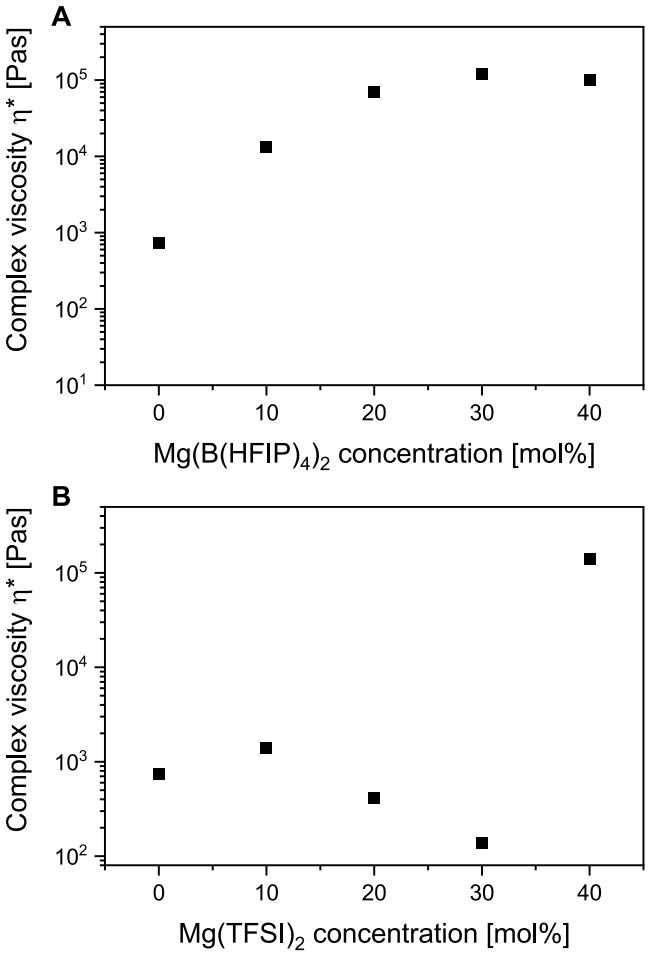

Figure 6. Complex viscosity at 20 °C by DFS measurements at γ_0 = 10% and ω = 0.32 rad s^{-1} for the given salt concentrations: (A) $Mg(B(HFIP)_4)_2$ and (B) $Mg(TFSI)_2$.

The large discrepancy between **TFSI40** and **TFSI30** may also be attributed to the formation of a polymer-in-salt situation, despite the lack of a sharp decrease in T_g.

Further structural information can be found by interpreting the DFS experiments (Figure 5B,D), where the corresponding slopes of linear fits for the parallel regime are given in Table S2. For an ideal cross-linked system, a linear behavior between angular frequency and storage and loss moduli with a slope of −1 would be expected; however, with slopes ranging between −0.67 and −1.50 in the parallel area, a nonideal behavior seems to be present. For the PEs containing $Mg(TFSI)_2$, in the frequency range mentioned before, G' and G'' cross each other with increasing salt concentration, resulting in a close parallel behavior, which is indicative of a structured material.[57] The crossover appearing for **TFSI40** at the highest frequency hints at entangled chains.[58] A parallel behavior of G' and G'' can also be seen by incorporating $Mg(B(HFIP)_4)_2$ instead of $Mg(TFSI)_2$, where parallel regimes can be seen for **HFIP20** and high salt concentrations. Those (**HFIP20**, **HFIP30**, and **HFIP40**) showed crossovers of G' and G'' at 452 rad s^{-1}, indicating dominantly elastic properties at higher frequencies, which were salt concentration independent. Moreover, for **HFIP20** a second low-frequency crossover of G' and G'' was found, whereas for the other samples, as e.g., **HFIP30**, a further crossover was indicated to occur at lower frequencies outside of the experimental frequency window. In the literature, such observations were explained by the formation of supramolecular dendritic aggregates of hydrogen-bonded supramolecular polymer networks.[59] Transferring this explanation to our system, a supramolecular ordered structure of Mg^{2+} coordinated and elongated polymers may be present. The observation of the second crossover of G' and G'' for **HFIP20** at the highest frequency of all samples next to the assumption of entangled polymers by parallel G' and G'' leads to the suggestion that for **HFIP20** the strongest interactions between the entangled polymers were present. The interactions related to this second crossover were assumed to be based on ionic interactions, including quasi-ionic cross-linking, and would therefore be reduced with increasing Mg-anion coordination or increasing distances between the elongated polymers. The quasi-ionic cross-linking was lower for **HFIP5** due to lower Mg^{2+} ion content, whereas for **HFIP30** and **HFIP20** the quasi-ionic cross-linking was decreased by the increasing separation of the polymers due to the higher salt content.

Impedance Spectroscopy. Ionic conductivity (σ) measurements were performed between −20 to 120 °C and further analyzed by fitting to the Vogel−Tammann−Fulcher (VTF) equation, presented as eq 1, where the A_0 factor is related to the number of mobile charge carriers and B is the pseudo activation energy of segmental mobility. T_0 is the Vogel temperature and can be estimated for a nonideal glass as $T_0 = T_g - 50$ °C. The VTF equation is commonly found to fit the temperature-dependent ionic conductivity for polymer electrolytes, where the ion mobility is influenced by the segmental motion of the polymer host.[60]

$$\sigma = A_0 \exp\left(-\frac{B}{R(T - T_0)}\right) \quad (1)$$

For VFT analysis, the results were plotted as $\ln(\sigma)$ against $(T - T_0)^{-1}$, as presented in Figure S12 and Table 2. For **TFSI5** to **TFSI40**, the ionic conductivity measurements resulted in maxima values of 2.7×10^{-7} S cm^{-1} for **TFSI5** at 20 °C followed by **TFSI20** with 6.4×10^{-9}, **TFSI30** with 1.0×10^{-9}, and **TFSI40** with 5.4×10^{-10} S cm^{-1} at 20 °C. At 120 °C, the maxima ionic conductivity changed its order toward **TFSI20** followed by **TFSI5**, **TFSI40**, and **TFSI30** (10^{-5} S cm^{-1}). The decreasing ionic conductivity with increasing $Mg(TFSI)_2$ concentration at 20 °C might be traced back to the aggregation of ions and the formation of ion clusters, as reported for PEO-based PEs before.[61] An explanation of the higher ionic conductivity of **TFSI20** and **TFSI40** over **TFSI5** and **TFSI30** at 120 °C is suggested by B and A_0. **TFSI40** and **TFSI20** were indicated to have a higher number of mobile charge carriers, leading to higher ion conductivities at 120 °C. In contrast to this,

Table 2. Parameters T_0, A_0, and B from the VTF Plot for TFSI5 to TFSI40 and HFIP5 to HFIP40

	T_0 [K]	A_0 [S cm^{-1} K^{-1}]	B [J mol^{-1} K^{-1}/eV]
TFSI5	216.35	0.003 ± 0.0006	5 872/0.14 ± 158/0.002
TFSI20	205.05	0.2 ± 0.05	12 487/0.15 ± 246/0.003
TFSI30	205.75	0.04 ± 0.02	12 511/0.15 ± 324/0.003
TFSI40	205.35	0.08 ± 0.04	13 247/0.17 ± 508/0.005
HFIP5	214.15	0.0007 ± 0.0002	13 319/0.06 ± 202/0.002
HFIP20	211.15	0.003 ± 0.0006	14 330/0.13 ± 217/0.002
HFIP30	211.55	0.0005 ± 0.0002	14 746/0.13 ± 98/0.001
HFIP40	181.15	2.78 ± 0.24	16 223/0.14 ± 98/0.001

https://doi.org/10.1021/acsomega.3c00761
ACS Omega 2023, 8, 23510−23520

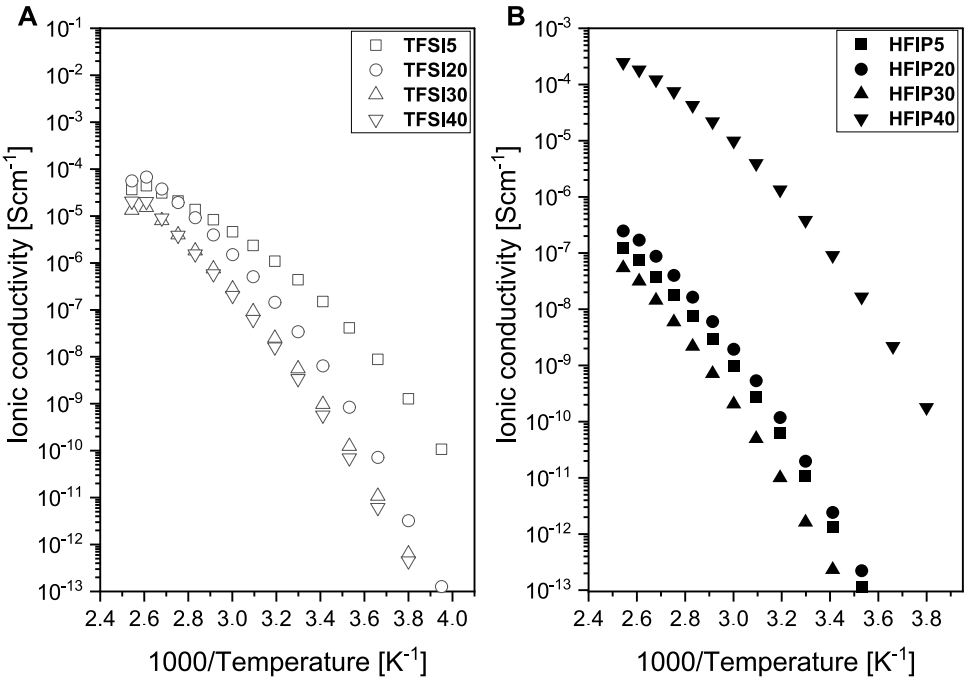

Figure 7. Temperature-dependent conductivity measurements between −20 to 120 °C of (A) **TFSI5** to **TFSI40** and (B) **HFIP5** to **HFIP40**.

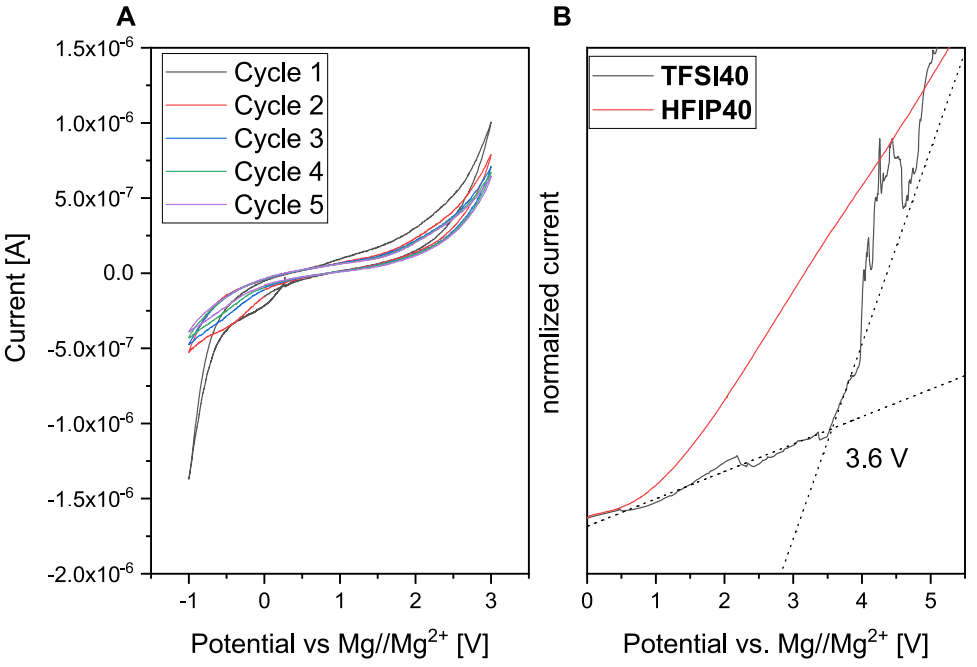

Figure 8. (A) Cyclic voltammetry of **HFIP40** in asymmetric Mg||SS cell at 80 °C and 0.1 mV s^{-1} between −2 to 2 V. (B) Electrochemical stability window in Mg||SS cell of **HFIP40** and **TFSI40** at 0.1 mV s^{-1} between 0 to 6 V.

the activation energy for segmental motion B seems to be more dominant at lower temperatures, explaining the higher ionic conductivity of **TFSI5** and **TFSI20**.

On changing the focus from $Mg(TFSI)_2$ to $Mg(B(HFIP)_4)_2$, the ionic conductivity increased for the PEs with increasing salt concentration, where **HFIP5** to **HFIP20** exhibited ionic conductivities in the same order of magnitude. In contrast, **HFIP40** exhibited substantially higher (about 3 orders of magnitude higher) ionic conductivity over the complete temperature range of −20 to 120 °C, between 1.8×10^{-10} and 2.5×10^{-4} S cm^{-1}. The significant difference in ionic conductivity for **HFIP40** again hints at the formation of a polymer-in-salt electrolyte. The curvature can be observed in Figure 7 for all of the temperature-dependent ionic conductivity data, so VTF plot analysis was conducted for all samples as shown in Figure S12. For the linearization of the VTF plots, only points for $T > 10$ °C were considered because at $T < T_g$ immobilization of polymer chains hinders ion mobility segmental motion. Overall, **HFIP5** to **HFIP20** showed in the VTF plots similar values for B and A_0, explaining the overall similar performance. But in the case of **HFIP40**, A_0 was several orders of magnitudes higher than for **HFIP30** (2.78 S cm^{-1} K^{-1}

https://doi.org/10.1021/acsomega.3c00761
ACS Omega 2023, 8, 23510−23520

compared to 0.0005 S cm^{-1} K^{-1}). Such an increase in the number of mobile charge carriers could be explained by the lower T_g of **HFIP40** being 30 °C below **HFIP30**. The high number of mobile charge carriers was also reported in a publication dealing with polymer-in-salt electrolytes, where for PAN copolymers a dramatic increase in ionic conductivity was described.[50] Furthermore, on comparing $Mg(B(HFIP)_4)_2$ to $Mg(TFSI)_2$-based PEs, the higher ionic conductivity for the $Mg(TFSI)_2$ electrolytes, except in the case of **HFIP40**, can be seen, explained by their lower η^*.

The ionic conductivity of **TFSI40** was in a similar range as the PCl-PTMC electrolytes containing $Mg(TFSI)_2$, with a maximum of 10^{-4} to 10^{-5} S cm^{-1} (36 mol % $Mg(TFSI)_2$) at 120 °C or PEC with 6×10^{-6} S cm^{-1} (40 mol % $Mg(TFSI)_2$) at 90 °C.[33,34] The higher ionic conductivity of **HFIP40** compared to the $Mg(TFSI)_2$-based electrolytes could enable higher plating and stripping efficiencies and was therefore of major interest in the following plating and stripping experiments.

Electrochemical Measurements. For the 40 mol %-containing PEs, **TFSI40** and **HFIP40**, the electrochemical stability window was tested against the magnesium metal by LSV on asymmetric Mg||SS cells. The results in Figures 8 and S13 show a much lower oxidative stability for **TFSI40**, which decomposed already at 3.6 V vs Mg/Mg^{2+} compared with **HFIP40** that did not show any decomposition behavior up to 5.5 V vs Mg/Mg^{2+}. The low stability of **TFSI40** might be because of the ionic aggregates and ion pairs, which are unstable against magnesium metal.[62,63] Wu and colleagues reported in 2021 for an LiTFSI-rich PE based on PEG ([EO/Li] = 0.5) also a decline in oxidation stability compared to lower concentrations.[64] The stability window of **HFIP40** was also larger than the reported potential for 1 M $Mg(B(HFIP)_4)_2$ in DME solution reported in 2018 (4 V).[39] Further, a higher stability for $Mg(B(HFIP)_4)_2$ over $Mg(TFSI)_2$-containing electrolytes was expected based on a prior publication.[38] Therefore, cyclic voltammetry measurements were performed for **HFIP40** on an asymmetric Mg||SS cell between −1 and 3 V, as presented in Figure 8. A decrease in current with cycle number and a lack of stripping-plating peaks were observed, attributed to the formation of a passivation layer on the magnesium surface. The growth and formation of the passivation layer was also detected by impedance spectroscopy before and after cyclic voltammetry, where an increase in surface resistance (R_s) was measured (Figure S13). Moreover, R_b seems to be quite high, being an argument for the low cyclability and the strong decrease in current. Therefore, and because of the low cyclability, our results do not support the idea of an enhanced performance of the $Mg(B(HFIP)_4)_2$-based polymer-in-salt electrolyte with regard to Mg plating or stripping efficiency.

CONCLUSIONS

Here, we prepared and characterized polycarbonate-based PEs containing P(BEC) as the polymer matrix and either $Mg(TFSI)_2$ or $Mg(B(HFIP)_4)_2$ salt. We showed the differing impact of anion character on the ion pair dissociation and agglomeration behavior and the polymer-Mg coordination, especially at high concentrations of 40 mol % magnesium salts (**TFSI40** and **HFIP40**). The incorporation of $Mg(TFSI)_2$ led to the formation of mainly polymer-Mg complexes at low concentrations, followed by a substantial increase of polymer-Mg-TFSI complexes with increasing $Mg(TFSI)_2$ concentration. Nevertheless, outside of the rheological measurements, the overall behavior of **TFSI40** was like that of a salt-in-polymer.

The incorporation of $Mg(B(HFIP)_4)_2$ led to salt-in-polymer electrolyte behavior at lower concentrations but polymer-in-salt behavior at 40 mol %. **HFIP40** exhibited the highest ionic conductivity (2.5×10^{-4} S cm^{-1} at 120 °C) among all samples and was found to have a higher oxidative (>5 V) stability than **TFSI40** (4.7 V). Still, **HFIP40** was not found to reversibly plate and strip magnesium metal. Therefore, use of this electrolyte with a magnesium anode may require use of artificial SEI to prevent anode passivation.

ASSOCIATED CONTENT

Supporting Information

The Supporting Information is available free of charge at https://pubs.acs.org/doi/10.1021/acsomega.3c00761.

List of ^{1}H NMR spectra (Figures S1−S5, Figures S10 and S11), DSC spectra (Figures S6 and S7), molar mass distribution (Figure S8), TGA spectra (Figure S9), Raman peak ratios of **TFSI40** to **TFSI5** (Table S1), Gradients of G' and G'' from DFS experiments (Table S2), VTF plots of the **TFSI5**/**HFIP5** to **TFSI40**/**HFIP40** (Figure S12), EIS spectra before and after CV of **HFIP40** (Figure S13)(PDF)

AUTHOR INFORMATION

Corresponding Author

Patrick Théato − *Institute for Chemical Technology and Polymer Chemistry, Karlsruhe Institute of Technology (KIT), D-76131 Karlsruhe, Germany; Institute for Biological Interfaces III, Karlsruhe Institute of Technology (KIT), D-76344 Eggenstein-Leopoldshafen, Germany;* orcid.org/0000-0002-4562-9254; Email: patrick.theato@kit.edu

Authors

David A. Sundermann − *Institute for Chemical Technology and Polymer Chemistry, Karlsruhe Institute of Technology (KIT), D-76131 Karlsruhe, Germany;* orcid.org/0000-0003-3091-4674

Bumjun Park − *College of Engineering, University of Notre Dame, Notre Dame, Indiana 46556, United States;* orcid.org/0000-0002-3779-1315

Valerian Hirschberg − *Institute for Chemical Technology and Polymer Chemistry, Karlsruhe Institute of Technology (KIT), D-76131 Karlsruhe, Germany;* orcid.org/0000-0001-8752-930X

Jennifer L. Schaefer − *College of Engineering, University of Notre Dame, Notre Dame, Indiana 46556, United States;* orcid.org/0000-0003-4293-6328

Complete contact information is available at: https://pubs.acs.org/10.1021/acsomega.3c00761

Funding

This work contributes to the research performed at CELEST (Center for Electrochemical Energy Storage Ulm-Karlsruhe) and was funded by the German Research Foundation (DFG) under Project ID 390874152 (POLiS Cluster of Excellence). Researchers at the University of Notre Dame thank the National Science Foundation for financial support via grant CBET-2044386.

Notes

The authors declare no competing financial interest.

■ ACKNOWLEDGMENTS

The authors thank the ND Energy Materials Characterization Facility (MCF) for the use of the Raman microscope. The MCF is funded by the Sustainable Energy Initiative (SEI), which is part of the Center for Sustainable Energy at Notre Dame (ND Energy).

■ REFERENCES

(1) Chen, T.; Jin, Y.; Lv, H.; Yang, A.; Liu, M.; Chen, B.; Xie, Y.; Chen, Q. Applications of Lithium-Ion Batteries in Grid-Scale Energy Storage Systems. *Trans. Tianjin Univ.* **2020**, *26*, 208−217.

(2) Trahey, L.; Brushett, F. R.; Balsara, N. P.; Ceder, G.; Cheng, L.; Chiang, Y.; Hahn, N. T.; Ingram, B. J.; Minteer, S. D.; Moore, J. S.; Mueller, K. T.; Nazar, L. F.; Persson, K. A.; Siegel, D. J.; Xu, K.; Zavadil, K. R.; Srinivasan, V.; Crabtree, G. W. Energy storage emerging: A perspective from the Joint Center for Energy Storage Research. *Proc. Natl. Acad. Sci. U.S.A.* **2020**, *117*, 12550−12557.

(3) Evarts, E. C. To the limits of lithium. *Nature* **2015**, *526*, 93−95.

(4) Lei, X.; Liang, X.; Yang, R.; Zhang, F.; Wang, C.; Lee, C.-S.; Tang, Y. Rational Design Strategy of Novel Energy Storage Systems: Toward High-Performance Rechargeable Magnesium Batteries. *Small* **2022**, *18*, No. e2200418.

(5) Skundin, A. M.; Kulova, T. L.; Yaroslatsev, A. B. Sodium-Ion batteries (a Review). *Russ. J. Electrochem.* **2018**, *54*, 113−151.

(6) Rajagopalan, R.; Tang, Y.; Ji, X.; Jia, C.; Wang, H. Advancements and Challenges in Potassium Ion Batteries: A Comprehensive Review. *Adv. Funct. Mater.* **2020**, *30*, No. 1909486.

(7) Mohtadi, R.; Tutusaus, O.; Arthur, T. S.; Zhao-Karger, Z.; Fichtner, M. The metamorphosis of rechargeable magnesium batteries. *Joule* **2021**, *5*, 581−617.

(8) Yoo, H. D.; Shterenberg, I.; Gofer, Y.; Gershinsky, G.; Pour, N.; Aurbach, D. Mg rechargeable batteries: an on-going challenge. *Energy Environ. Sci.* **2013**, *6*, 2265.

(9) Bella, F.; de Luca, S.; Fagiolari, L.; Versaci, D.; Amici, J.; Francia, C.; Bodoardo, S. An Overview on Anodes for Magnesium Batteries: Challenges towards a Promising Storage Solution for Renewables. *Nanomaterials* **2021**, *11*, No. 810.

(10) Ehrenberger, S.; Friedrich, H. E. Life-Cycle Assessment of the Recycling of Magnesium Vehicle Components. *JOM* **2013**, *65*, 1303−1309.

(11) UNEP − International Resource Panel. *Report 2: Recycling Rates of Metals − A Status Report*.

(12) Kuwata, H.; Matsui, M.; Imanishi, N.; et al. Passivation Layer Formation of Magnesium Metal Negative Electrodes for Rechargeable Magnesium Batteries. *J. Electrochem. Soc.* **2017**, *164*, A3229.

(13) Levi, E.; Levi, M. D.; Chasid, O.; Aurbach, D. A review on the problems of the solid state ions diffusion in cathodes for rechargeable Mg batteries. *J. Electroceram.* **2009**, *22*, 13−19.

(14) Xue, X.; Chen, R.; Song, X.; Tao, A.; Yan, W.; Kong, W.; Jin, Z. Electrochemical Mg 2+ Displacement Driven Reversible Copper Extrusion/Intrusion Reactions for High-Rate Rechargeable Magnesium Batteries. *Adv. Funct. Mater.* **2021**, *31*, No. 2009394.

(15) Park, B.; Schaefer, J. L. Review—Polymer Electrolytes for Magnesium Batteries: Forging Away from Analogs of Lithium Polymer Electrolytes and Towards the Rechargeable Magnesium Metal Polymer Battery. *J. Electrochem. Soc.* **2020**, *167*, No. 070545.

(16) Sharma, J.; Hashmi, S. A. Plastic crystal-incorporated magnesium ion conducting gel polymer electrolyte for battery application. *Bull Mater Sci* **2018**, *41*, 1623.

(17) Kumar, G. G.; Munichandraiah, N. Effect of plasticizers on mangeisum-poly(ethylenoxide) electrolyte. *J. Electroanal. Chem.* **2000**, *495*, 42−50.

(18) Jeong, S.-K.; Jo, Y.-K.; Jo, N.-J. Decoupled ion conduction mechanism of poly(vinyl alcohol) based Mg-conducting solid polymer electrolyte. *Electrochim. Acta* **2006**, *52*, 1549−1555.

(19) Kumar, G. G.; Munichandraiah, N. Poly(methylmethacryalte) - magnesium triflate gel polymer electrolyte for solid state magensium battery application. *Electrochim. Acta* **2002**, *47*, 1013−1022.

(20) Sun, B.; Mindemark, J.; Edström, K.; Brandell, D. Polycarbonate-based solid polymer electrolytes for Li-ion batteries. *Solid State Ionics* **2014**, *262*, 738−742.

(21) Sun, B.; Mindemark, J.; V Morozov, E.; Costa, L. T.; Bergman, M.; Johansson, P.; Fang, Y.; Furó, I.; Brandell, D. Ion transport in polycarbonate based solid polymer electrolytes: experimental and computational investigations. *Phys. Chem. Chem. Phys.* **2016**, *18*, 9504−9513.

(22) Sun, B.; Mindemark, J.; Edström, K.; Brandell, D. Realization of high performance polycarbonate-based Li polymer batteries. *Electrochem. Commun.* **2015**, *52*, 71−74.

(23) Wang, Q.; Liu, X.; Cui, Z.; Shangguan, X.; Zhang, H.; Zhang, J.; Tang, K.; Li, L.; Zhou, X.; Cui, G. A fluorinated polycarbonate based all solid state polymer electrolyte for lithium metal batteries. *Electrochim. Acta* **2020**, *337*, No. 135843.

(24) Sångeland, C.; Younesi, R.; Mindemark, J.; Brandell, D. Towards room temperature operation of all-solid-state Na-ion batteries through polyester−polycarbonate-based polymer electrolytes. *Energy Storage Mater.* **2019**, *19*, 31−38.

(25) Mindemark, J.; Mogensen, R.; Smith, M. J.; Silva, M. M.; Brandell, D. Polycarbonates as alternative electrolyte host materials for solid-state sodium batteries. *Electrochem. Commun.* **2017**, *77*, 58−61.

(26) Morioka, T.; Ota, K.; Tominaga, Y. Effect of oxyethylene side chains on ion-conductive properties of polycarbonate-based electrolytes. *Polymer* **2016**, *84*, 21−26.

(27) Ebadi, M.; Eriksson, T.; Mandal, P.; Costa, L. T.; Araujo, C. M.; Mindemark, J.; Brandell, D. Restricted Ion Transport by Plasticizing Side Chains in Polycarbonate-Based Solid Electrolytes. *Macromolecules* **2020**, *53*, 764−774. Published Online: Jan. 31, 2020.

(28) Matsumoto, M.; Uno, T.; Kubo, M.; Itoh, T. Polymer electrolytes based on polycarbonates and their electrochemical and thermal properties. *Ionics* **2013**, *19*, 615−622.

(29) Zhang, J.; Yang, J.; Dong, T.; Zhang, M.; Chai, J.; Dong, S.; Wu, T.; Zhou, X.; Cui, G. Aliphatic Polycarbonate-Based Solid-State Polymer Electrolytes for Advanced Lithium Batteries: Advances and Perspective. *Small* **2018**, *14*, No. e1800821.

(30) Soo, P. P.; Huang, B.; Jang, Y.-I.; Chiang, Y.-M.; Sadoway, D. R.; Mayes, A. M. Rubbery Block Copolymer Electrolytes for Solid-State Rechargeable Lithium Batteries. *J. Electrochem. Soc.* **1999**, *146*, 32−37.

(31) Tominaga, Y.; Shimomura, T.; Nakamura, M. Alternating copolymers of carbon dioxide with glycidyl ethers for novel ion-conductive polymer electrolytes. *Polymer* **2010**, *51*, 4295−4298.

(32) Zhang, J.; Zhao, J.; Yue, L.; Wang, Q.; Chai, J.; Liu, Z.; Zhou, X.; Li, H.; Guo, Y.; Cui, G.; Chen, L. Safety-Reinforced Poly(Propylene Carbonate)-Based All-Solid-State Polymer Electrolyte for Ambient-Temperature Solid Polymer Lithium Batteries. *Adv. Energy Mater.* **2015**, *5*, No. 1501082.

(33) Park, B.; Andersson, R.; Pate, S. G.; Liu, J.; O'Brien, C. P.; Hernández, G.; Mindemark, J.; Schaefer, J. L. Ion Coordination and Transport in Magnesium Polymer Electrolytes Based on Polyester-co-Polycarbonate. *Energy Mater. Adv.* **2021**, *2021*, No. 9895403.

(34) Ab Aziz, A.; Tominaga, Y. Magnesium ion-conductive poly(ethylene carbonate) electrolytes. *Ionics* **2018**, *24*, 3475−3481.

(35) Kuwata, H.; Matsui, M.; Imanishi, N. Passivation Layer Formation of Magnesium Metal Negative Electrodes for Rechargeable Magnesium Batteries. *J. Electrochem. Soc.* **2017**, *164*, A3229−A3236.

(36) Alwast, D.; Schnaidt, J.; Hancock, K.; Yetis, G.; Behm, R. J. Effect of Li + and Mg 2+ on the Electrochemical Decomposition of the Ionic Liquid 1-Butyl-1- methylpyrrolidinium bis(trifluoromethanesulfonyl)-imide and Related Electrolytes. *ChemElectroChem* **2019**, *6*, 3009−3019.

(37) Liu, Y.; Yu, P.; Wu, Y.; Yang, H.; Xie, M.; Huai, L.; Goddard, W. A.; Cheng, T. The DFT-ReaxFF Hybrid Reactive Dynamics Method with Application to the Reductive Decomposition Reaction of the TFSI and DOL Electrolyte at a Lithium-Metal Anode Surface. *J. Phys. Chem. Lett.* **2021**, *12*, 1300−1306.

(38) Tuerxun, F.; Yamamoto, K.; Mandai, T.; Tateyama, Y.; Nakanishi, K.; Uchiyama, T.; Watanabe, T.; Tamenori, Y.; Kanamura, K.; Uchimoto, Y. Effect of Interaction among Magnesium

https://doi.org/10.1021/acsomega.3c00761
ACS Omega 2023, 8, 23510−23520

Ions, Anion, and Solvent on Kinetics of the Magnesium Deposition Process. *J. Phys. Chem. C* **2020**, *124*, 28510−28519.
(39) Zhao-Karger, Z.; Liu, R.; Dai, W.; Li, Z.; Diemant, T.; Vinayan, B. P.; Bonatto Minella, C.; Yu, X.; Manthiram, A.; Behm, R. J.; Ruben, M.; Fichtner, M. Toward Highly Reversible Magnesium−Sulfur Batteries with Efficient and Practical Mg[B(hfip) 4] 2 Electrolyte. *ACS Energy Lett.* **2018**, *3*, 2005−2013.
(40) Jankowski, P.; Li, Z.; Zhao-Karger, Z.; Diemant, T.; Fichtner, M.; Vegge, T.; Lastra, J. M. G. Development of Magnesium Borate Electrolytes: Explaining the Success of Mg[B(hfip)4]2 Salt. *Energy Storage Mater.* **2022**, *45*, 1133−1143.
(41) Long, L.; Wang, S.; Xiao, M.; Meng, Y. Polymer electrolytes for lithium polymer batteries. *J. Mater. Chem. A* **2016**, *4*, 10038−10069.
(42) Ferry, A.; Edman, L.; Forsyth, M.; MacFarlane, D. R.; Sun, J. Connectivity, ionic interactions, and migration in a fast-ion-conducting polymer-in-salt electrolyte based on poly(acrylonitrile) and LiCF3SO3. *J. Appl. Phys.* **1999**, *86*, 2346−2348.
(43) Mishra, R.; Baskaran, N.; Ramakrishnan, P. A.; Rao, K. J. Lithium ion conduction in extreme polymer in salt regime. *Solid State Ionics* **1998**, *112*, 261−273.
(44) Bushkova, O. V.; Zhukovsky, V. M.; Lirova, B. I.; Kruglyashov, A. L. Fast ionic transport in solid polymer electrolytes based on acrylonitrile copolymers. *Solid State Ionics* **1999**, *119*, 217−222.
(45) Łasińska, A.; Marzantowicz, M.; Dygas, J. R.; Krok, F.; Florjańczyk, Z.; Tomaszewska, A.; Zygadło-Monikowska, E.; Żukowska, Z.; Lafont, U. Study of ageing effects in polymer-in-salt electrolytes based on poly(acrylonitrile-co-butyl acrylate) and lithium salts. *Electrochim. Acta* **2015**, *169*, 61−72.
(46) Wang, Z.; Gao, W.; Chen, L.; Mo, Y.; Huang, X. Study on roles of polyacrylonitrile in 'salt-in-polymer" and 'polymer-in-salt" electrolytes. *Solid State Ionics* **2002**, 51−56.
(47) He, P.; Ford, H. O.; Gonzalez, S.; Rodriguez, S.; Oliver, A. G.; Schaefer, J. L. Stability and Disproportionation of Magnesium Polysulfides and the Effects on the Mg-Polysulfide Flow Battery. *J. Electrochem. Soc.* **2021**, *168*, No. 110516.
(48) Dove, A. P.; Pratt, R. C.; Lohmeijer, B. G. G.; Waymouth, R. M.; Hedrick, J. L. Thiourea-based bifunctional organocatalysis: supramolecular recognition for living polymerization. *J. Am. Chem. Soc.* **2005**, *127*, 13798−13799.
(49) Butzelaar, A. J.; Röring, P.; Mach, T. P.; Hoffmann, M.; Jeschull, F.; Wilhelm, M.; Winter, M.; Brunklaus, G.; Théato, P. Styrene-Based Poly(ethylene oxide) Side-Chain Block Copolymers as Solid Polymer Electrolytes for High-Voltage Lithium-Metal Batteries. *ACS Appl. Mater. Interfaces* **2021**, *13*, 39257−39270.
(50) Florjańczyk, Z.; Zygadło-Monikowska, E.; Wieczorek, W.; Ryszawy, A.; Tomaszewska, A.; Fredman, K.; Golodnitsky, D.; Peled, E.; Scrosati, B. Polymer-in-Salt Electrolytes Based on Acrylonitrile/Butyl Acrylate Copolymers and Lithium Salts. *J. Phys. Chem. B* **2004**, *108*, 14907−14914.
(51) Rey, I.; Johansson, P.; Lindgren, J.; Lassègues, J. C.; Grondin, J.; Servant, L. Spectroscopic and Theoretical Study of (CF3SO2)2N-(TFSI-) and (CF3SO2)NH (HTFSI). *J. Phys. Chem. A* **1998**, *102*, 3249−3258.
(52) Shao, Y.; Rajput, N. N.; Hu, J.; Hu, M.; Liu, T.; Wei, Z.; Gu, M.; Deng, X.; Xu, S.; Han, K. S.; Wang, J.; Nie, Z.; Li, G.; Zavadil, K. R.; Xiao, J.; Wang, C.; Henderson, W. A.; Zhang, J.-G.; Wang, Y.; Mueller, K. T.; Persson, K.; Liu, J. Nanocomposite polymer electrolyte for rechargeable magnesium batteries. *Nano Energy* **2015**, *12*, 750−759.
(53) Wheatle, B. K.; Lynd, N. A.; Ganesan, V. Effect of Polymer Polarity on Ion Transport: A Competition between Ion Aggregation and Polymer Segmental Dynamics. *ACS Macro Lett.* **2018**, *7*, 1149−1154.
(54) Raghavan, S. R.; Riley, M. W.; Fedkiw, P. S.; Khan, S. A. Composite Polymer Electrolytes Based on Poly(ethylene glycol) and Hydrophobic Fumed Silica: Dynamic Rheology and Microstructure. *Chem. Mater.* **1998**, *10*, 244−251.
(55) Earnest, T. R.; Macknight, W. J. Effect of hydrogen bonding and ionic aggregation on the melt rheology of an ethylene−methacrylic acid copolymer and its sodium salt. *J. Polym. Sci., Polym. Phys. Ed.* **1978**, *16*, 143−157.
(56) Takahashi, T.; Watanabe, J.; Minagawa, K.; Koyama, K. Effect of ionic interaction on elongational viscosity of ethylene-based ionomer melts. *Polymer* **1994**, *35*, 5722−5728.
(57) Dintcheva, N. T.; Furlani, M.; Jayasundara, W. J. M. J. S. R.; Bandara, T. M. W. J.; Mellander, B.-E.; La Mantia, F. P. Rheological behavior of PAN-based electrolytic gel containing tetrahexylammonium and magnesium iodide for photoelectrochemical applications. *Rheol. Acta* **2013**, *52*, 881−889.
(58) Larson, G. *The Structure and Rheology of Complex Fluids*, Illustrated edition; Oxford University Press, 1998.
(59) Chen, S.; Döhler, D.; Binder, W. H. Rheology of hydrogen-bonded dendritic supramolecular polymer networks in the melt state. *Polymer* **2016**, *107*, 466−473.
(60) Girish Kumar, G.; Munichandraiah, N. Effect of plasticizers on magnesium-poly(ethyleneoxide) polymer electrolyte. *J. Electroanal. Chem.* **2000**, *495*, 42−50.
(61) Jaipal Reddy, M.; Chu, P. P. Ion pair formation and its effect in PEO:Mg solid polymer electrolyte system. *J. Power Sources* **2002**, *109*, 340−346.
(62) Baskin, A.; Prendergast, D. Exploration of the Detailed Conditions for Reductive Stability of Mg(TFSI) 2 in Diglyme: Implications for Multivalent Electrolytes. *J. Phys. Chem. C* **2016**, *120*, 3583−3594.
(63) Rajput, N. N.; Qu, X.; Sa, N.; Burrell, A. K.; Persson, K. A. The coupling between stability and ion pair formation in magnesium electrolytes from first-principles quantum mechanics and classical molecular dynamics. *J. Am. Chem. Soc.* **2015**, *137*, 3411−3420.
(64) Wu, H.; Gao, P.; Jia, H.; Zou, L.; Zhang, L.; Cao, X.; Engelhard, M. H.; Bowden, M. E.; Ding, M. S.; Hu, J.; Hu, D.; Burton, S. D.; Xu, K.; Wang, C.; Zhang, J.-G.; Xu, W. A Polymer-in-Salt Electrolyte with Enhanced Oxidative Stability for Lithium Metal Polymer Batteries. *ACS Appl. Mater. Interfaces* **2021**, *13*, 31583−31593.

https://doi.org/10.1021/acsomega.3c00761
ACS Omega 2023, 8, 23510−23520